LAWRENCE
LIVERMORE
NATIONAL
LABORATORY

LLNL-JRNL-753963

E-band fiber laser performance and power analysis with longitudinally averaged population modeling

L. S. Kiani, R. J. Beach, J. W. Dawson, P. H. Pax, G. S. Allen, D. R. Drachenberg, V. V. Khitrov, N. Schenkel, M. J. Cook, R. P. Crist, M. J. Messerly

June 29, 2018

Journal of the Optical Society of America B

Disclaimer

This document was prepared as an account of work sponsored by an agency of the United States government. Neither the United States government nor Lawrence Livermore National Security, LLC, nor any of their employees makes any warranty, expressed or implied, or assumes any legal liability or responsibility for the accuracy, completeness, or usefulness of any information, apparatus, product, or process disclosed, or represents that its use would not infringe privately owned rights. Reference herein to any specific commercial product, process, or service by trade name, trademark, manufacturer, or otherwise does not necessarily constitute or imply its endorsement, recommendation, or favoring by the United States government or Lawrence Livermore National Security, LLC. The views and opinions of authors expressed herein do not necessarily state or reflect those of the United States government or Lawrence Livermore National Security, LLC, and shall not be used for advertising or product endorsement purposes.

E-band fiber laser performance and power analysis with longitudinally averaged population modeling

LEILY S. KIANI, [1,*] RAYMOND J. BEACH, [1] JAY W. DAWSON, [1] PAUL H. PAX, [1] GRAHAM S. ALLEN, [1] DERREK R. DRACHENBERG, [1] VICTOR V. KHITROV, [1] NICK SCHENKEL, [1] MATTHEW J. COOK, [1] ROBERT P. CRIST [1] AND MICHAEL J. MESSERLY [1]

[1]*Publications Department, OSA—The Optical Society, 2010 Massachusetts Avenue N.W., Washington, D.C. 20036*
**Corresponding author: kiani2@llnl.gov*

Received XX Month XXXX; revised XX Month, XXXX; accepted XX Month XXXX; posted XX Month XXXX (Doc. ID XXXXX); published XX Month XXXX

To help facilitate the modeling of new fiber laser systems, such as those with complex functional microstructures, we report on a simplified modeling methodology that can accommodate the parasitic kinetic effects often present in such systems. The essence of our approach is to integrate over the length of the gain medium at the outset, thereby forfeiting longitudinally resolved information about the system but simplifying its energetics analysis. To illustrate the benefits of our new approach over more conventional coupled-rate-equation analyses we apply our model to a Nd^{3+} doped fiber laser operating on the $^4F_{3/2}$ - $^4I_{13/2}$ transition at 1400 nm. The model produces closed form solutions for the various output channels available to the pump power and enables projections of ultimate laser performance to be conveniently generated.

OCIS codes: *(140.3490) Lasers, distributed-feedback; (060.2420) Fibers, polarization-maintaining; (060.3735) Fiber Bragg gratings; (060.2370) Fiber optics sensors.*

http://dx.doi.org/10.1364/AO.99.099999

1. INTRODUCTION

A focus of recent work has been to understand the performance of fiber laser systems utilizing lasant transitions that have previously been inaccessible to laser action because of competition from stronger lasing transitions in the same lasant. The prospects for efficiently utilizing such weak transitions has improved dramatically with the ability to now engineer into photonic crystal fibers, shaped spectral filters capable of suppressing unwanted stronger transitions while simultaneously not introducing excessive loss on desired weaker transitions. This technology approach promises a renaissance in expanding the wavelength coverage of lasers and is being actively pursued by LLNL. With an eye toward optimizing such systems, investigative studies often involve trading off various system parameters such as spectral gain and loss characteristics of filters, glass compositions, and different lasant ions, and assessing the impact of various parasitic kinetic processes that can steal useful laser power such as excited state absorption and background scatter and/or absorption loss. Such studies are often initially carried out with rate-equation based models to narrow the parameter space that will be explored in an experimental investigation using, for example, a customized photonic crystal fiber.

To help facilitate the analysis of these systems, we here report on a methodology that we adapt to modeling fiber systems and which we believe offers substantial simplifications over the rate-equation based analyses that have typically been used for generating such models. The essence of our approach is to integrate over the length of the gain medium at the outset which simplifies the subsequent energetics analysis of the laser at the cost of losing longitudinally resolved information about the laser system. The model, originally developed for diode-pumped solid-state lasers and more recently applied to diode-pumped alkali lasers, is used here because we are primarily interested in the output characteristics of the laser and because of the ease with which parasitic kinetic effects such as excited state and background absorption can be handled.

There exist a few methods for spectrally filtering the light in a fiber core for the purpose inhibiting gain on an undesired lasant transition. Schemes using rare earth absorption such as that in samarium have been used to deplete spectrum for gain tailoring [1]. Optical fibers with a region of low index surrounding the core within the cladding region, referred to as W-type or trench index profile, have been developed for inducing loss the fundamental guided mode at long wavelengths. The design, originally intended for dispersion tailoring [2] induces loss at longer wavelengths due to the mode field expanding for longer wavelengths. As the mode field expands, the confinement losses grow, generating a longitudinal short-pass filter which can be used to filter gain [3].

Photonic crystal fibers are a general class of fibers where the dimensions of a lattice microstructure determine the waveguide properties. This technology allows for a variety of guiding and filtering schemes. In the photonic bandgap fibers (PBGF), guidance is based on a lattice structure but is strictly different than the guiding properties of the microstructure in this fiber. The photonic bandgap fibers, generate

bands of guidance where the relevant laser wavelengths operate. The tunability of the bandgap structure can be exploited to guide in a specific wavelength band and in this way the high loss at all other wavelengths can suppress unwanted amplification.

The spectrally filtering waveguide is a modification of the Photonic Crystal Fiber (PCF) design, which consists of a lattice of index depressions, with one or more defects (missing depressions) comprising the guiding core, the entire lattice being surrounded by pure fused silica. In contrast to guiding via bandgap effect, the microstructure we design is broadly guiding via modified total internal reflection with loss introduced via resonant coupling to raised index inclusions. This effectively constitutes a notch filtering mechanism where the resonant effects, which typically have spiky, narrow features as in the PGBFs, serve to introduce loss to unwanted transitions. The complicated features of the loss profile are not essential to the filtering effects so long as the lower-loss valleys between the high-loss peaks remain sufficiently lossy to suppress amplification in regions where spontaneous emission can occur. The photonic bandgap effect in fibers could be utilized for promoting gain on previously unused rare earth transitions but the constraints on the microstructure fabrication are stricter than that for the wavelength selective filtering microstructure presented here.

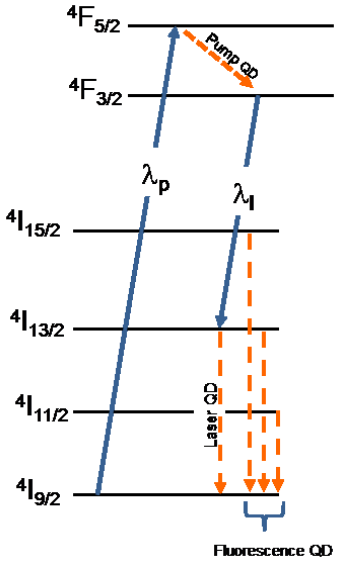

Figure1: Simplified energy level diagram of Nd^{3+} laser system showing the levels of interest for kinetics in the laser.

Active fibers producing gain on the $^4F_{3/2}$ to $^4I_{13/2}$ transition in Nd^{3+} have been attractive for decades driven mainly by telecommunications applications [4, 5]. This transition in has been extensively explored in solid state media [6] for example in YAG, YAlO, YVO, YGdVO [7] and in YAP [8]. Emission from this transition is difficult to promote in silica because of (1) strong competition from the 1060 nm and 920 nm emission peaks (i.e. low branching ratio of 0.1 [9]), (2) the coincidence of the energy gap for excited state absorption from the upper level laser state with the emission band [10] and (3) the water absorption peak at 1380 nm. Despite these inhibitors to lasing on this transition, the long interaction length in a fiber laser can have many emission events leading to significant amplification of light around 1400 nm. By introducing loss to other spectral bands through a distributed filter incorporated into the waveguide design, amplification of the spontaneous emission and thus competitive lasing in the 1060 nm and 920 nm bands is suppressed.

We present a spectrally filtering microstructure fiber laser operating on the $^4F_{3/2}$ to $^4I_{13/2}$ transition in Nd^{3+}. Section I gives a brief explanation of the waveguide design which is followed by the laser design and performance. Section II outlines the modeling approach and presents modeling results with a projection for a future improved fiber. Finally, we present a discussion of the outlook for wavelength selection in fiber lasers using this approach.

A. Waveguide Design

The basis of the filtering fiber is spectrally dependent reduction of core guidance, in this case brought on by auxiliary waveguide elements that form a bridge spanning the confining 'wall' surrounding the core [11]. The auxiliary elements are chosen to be resonant with the core at the wavelength to be filtered, so that light in the core couples to, and spreads into them. They are also chosen to have higher dispersion than the core so that the resonance is constricted to a limited spectral band. In our design, the core confinement 'wall' is a depressed index region. The core index is matched to that of pure silica with very low NA and waveguide dispersion. We replace several of the depressed index lattice sites with auxiliary high index inclusions, extending from near the core to the edge of the PCF lattice. The auxiliary elements are strings of graded-index (GRIN) waveguides with relatively high waveguide dispersion due to their high NA and small size. These GRINs are arranged six groups or 'spokes' of three inclusions. The GRINs support modes of their own, which are chosen to be resonant with the fundamental core mode at the wavelength we wish to filter; at resonance, the core mode couples to these inclusions. The outer cladding region is also pure silica. Crucially, because the core mode's effective index is below that of the surrounding fused silica, any light that couples to the resonant elements will be stripped to the region outside the lattice. That is, core guidance is lost when the resonance condition is satisfied.

B. Laser Design and Performance

The fiber, pictured in figure 2 (b), was fabricated by stacking millimeter size glass elements into a preform and drawing it down to 126.5 μm outer diameter with a pitch of 6.44 μm. The core material was obtained from Optacore SA as a Nd^{3+} doped glass rod co-doped with 0.75 mol % Al_2O_3. The core material showed 40 dB/m of absorption at 808 nm. Doped glass was matched to the index of silica by repeatedly stacking and drawing a mixture of doped canes with fluorinated glass canes of lower index, obtained from Prysmian. Absorption at the pump wavelength in the final fiber was 14.3 dB/m and core background loss was between 0.1 and 0.15 dB/m. Our approach to index matching of the doped core material to the index of silica to raises the background loss thus it interferes with the maximum achievable efficiency. Processing techniques to limit contamination and OH absorption during fabrication are being explored to address the increased background losses.

Figure 2 (a) shows the laser setup where two 7 m gain fibers are pumped bidirectionally with four 808 nm fiber coupled diode lasers (LUMICS LU808M250), each spliced on to one end of a custom-made wavelength division multiplexer (Gooch & Housego) for combination of 808 nm and 1400 nm. This length and configuration is chosen to avoid feedback of the pumps into one another because > 90% of the light from one pump laser is absorbed in 3.5 m of doped fiber. The combined pumps apply up to 888 mW of pump power to the system.

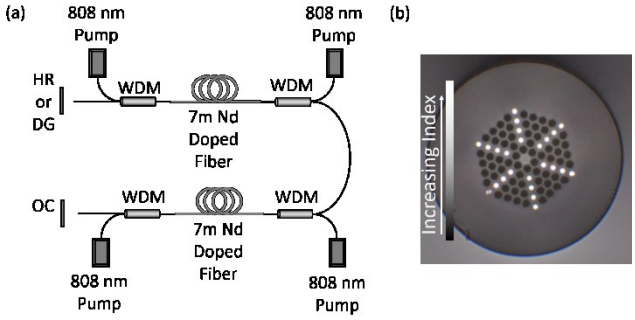

Figure 2: (a) diagram of fiber laser with two gain stages. Four custom-made wavelength division multiplexers (WDM) combine pumps with laser light in the doped fiber, high reflector (HR) or diffraction grating (DG) form the cavity with the output coupler (OC). (b) Picture of the transverse profile of the fabricated fiber. The fiber is solid microstructure fiber with dark regions corresponding to fluorinated regions of lower refractive index and brighter regions corresponding to areas of higher index formed by graded index (GRIN) inclusions to the microstructure lattice.

A high reflector with > 99% reflection at 1400 nm (Thorlabs BB1 E04) was placed at one end of the cavity and several output couplers with varying reflectivity were placed at the other end. Slope efficiencies for various output couplers ranging from 4% to 67% are plotted in figure 3 (a) with a maximum of 26%. In the tunable laser setup, the high reflector at one end of the cavity was replaced by a diffraction grating in the Littrow configuration. Feedback into the cavity is spectrally dependent and tuning is performed by rotating the diffraction grating.

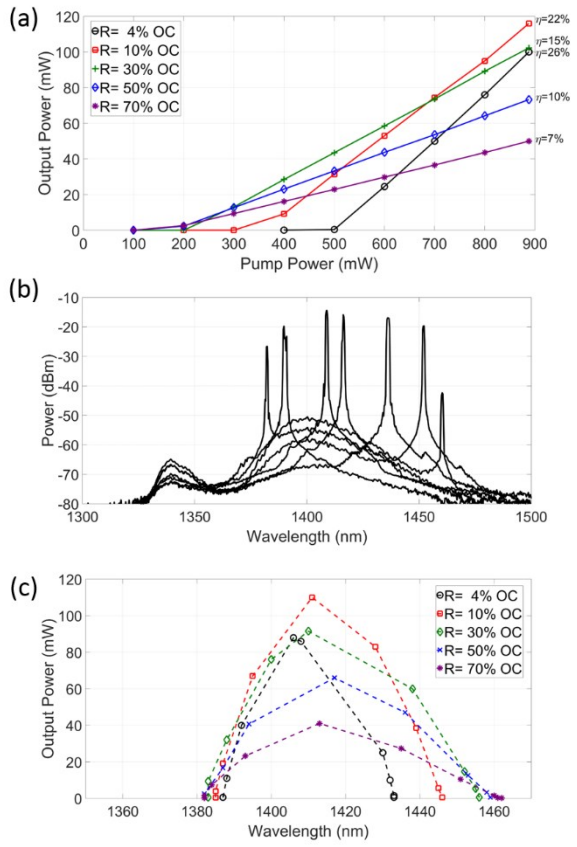

Figure 3: (a) Slope efficiencies for various output couplers showing a maximum slope efficiency of 26% (black circles) for the case where the fiber end cleave acts as an output coupler with 4% reflection. Lines are drawn between points to guide the eye. (b) Laser output spectrum with varied diffraction grating angle demonstrating tunability from 1382 nm to 1462 nm. (c) Tuning ranges for output couplers of various reflectivity.

The grating's diffraction efficiency measured at 1390 nm was found to be 65% to the first order beam. Figure 3 (b) shows spectra spanning the full tuning range for an output coupler with 67% reflectivity. The full gain spectrum for this optical fiber in an amplifier configuration was measured by seeding the gain stages with a 1390 nm laser operating below threshold which served as a broadband source [12]. Gain spectrum was measured to span a 90 nm window from 1373 nm to 1500 nm. Single pass system losses ranging from 2 to 4 dB across the gain spectrum were also measured with this source. Excited state absorption influences the achievable gain for wavelengths shorter than 1380 nm and pump induced losses were measured in the range between 1353 nm and 1376 nm. Losses limited the experimentally achievable laser tuning range to 80 nm between 1382 nm and 1462 nm shown in figure 3 (b). Measured tuning curves for various output couplers are shown in figure 3 (c) with the broadest tuning curve resulting from the highest feedback reflection at the output coupler of 67%. The 10 nm difference between the measured gain spectrum bandwidth and the achievable laser tuning is attributed to the relatively high loss in the cavity in the tunable laser configuration.

2. MODELING

To illustrate our modeling approach, we here apply it to the fiber laser system described above. Figure 1 shows the levels of interest of the Nd^{3+} ion. Population is pumped from the $^4I_{9/2}$ level to the $^4F_{5/2}$ level using 808 nm diode pumps. From the $^4F_{5/2}$ level the population rapidly decays non-radiatively to the $^4F_{3/2}$ level. Lasing action then transfers population from the $^4F_{3/2}$ level to the $^4I_{13/2}$ level via the stimulated emission of photons around 1400 nm. Lasing action on the stronger $^4F_{3/2}$-$^4I_{9/2}$ and $^4F_{3/2}$-$^4I_{11/2}$ transitions is frustrated using a spectral filter engineered into the photonic crystal structure. The population that transfers into the $^4I_{13/2}$ terminal laser level then rapidly decays back to the ground $^4I_{9/2}$ level non-radiatively. In addition to sourcing laser radiation, population that collects in the $^4F_{3/2}$ level can also be transferred to the higher lying $^2G_{7/2}$ level via excited state absorption (ESA) of laser photons at also around 1400 nm; a process that can steal useful laser power from the system and degrade overall system performance.

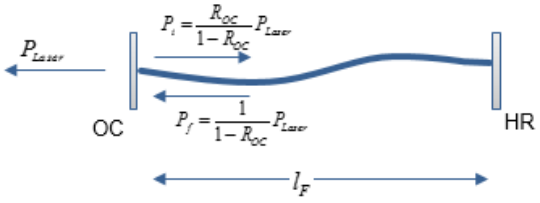

Figure 4: Schematic diagram of the laser system that is being modeled. The length of the fiber is l_f, OC denotes the output coupler and HR the high reflector. P_i denotes the intracavity power in the fiber just after reflecting off the OC, and P_f the intracavity laser power just prior to intercepting the OC. P_{laser} is the laser power that exits the output coupler.

Under the assumption that populations in all excited levels except the metastable $^4F_{3/2}$ initial laser level decay rapidly compared to the characteristic pump excitation and stimulated emission rates,

populations can be assumed negligible in all but the initial laser $^4F_{3/2}$ metastable level and the ground $^4I_{9/2}$ level. To simplify notation in what follows the ground $^4I_{9/2}$ level is denoted as level 1 and the metastable $^4F_{3/2}$ level as level 2. Figure 4 shows a sketch of the fiber laser system that we will use as a guide to set up our rate equation model.

The intracavity power evolving from stimulated emission events and reduced by absorption effects can be described as

$$\frac{dP(x)}{dx} = P(x)[\eta_{ol}(\sigma_{em} - \sigma_{ESA})n_2(x) - \alpha_{BG}] \quad (1)$$

where x denotes the longitudinal position in the fiber and ranges from 0 to $2l_f$. η_{ol} is the mode overlap of the laser irradiance profile in the fiber with the fiber's gain core, σ_{em} is the $^4F_{3/2}\rightarrow{}^4I_{13/2}$ stimulated emission cross section, σ_{ESA} is the excited state absorption cross section, $n_2(x)$ is the spatially dependent $^4F_{3/2}$ population density, and α_{BG} is the background absorption and scatter loss in the fiber. Integrating **Error! Reference source not found.** around the fiber gives

$$ln\left(\frac{P_f}{P_i}\right) = \int_0^{2l_f}[\eta_{ol}(\sigma_{em} - \sigma_{ESA})n_2(x) - \alpha_{BG}]\,dx \quad (2)$$

or

$$P_f = P_i e^{\int_0^{2l_f}[\eta_{ol}(\sigma_{em}-\sigma_{ESA})n_2(x)-\alpha_{BG}]dx} \quad (3)$$

The key to the longitudinally averaged population model under consideration here is to notice that in equation **Error! Reference source not found.**, if we make the replacement

$$\int_0^{2l_f} n_2\,(x)dx \longrightarrow \langle n_2\rangle 2l_f \quad (4)$$

where $\langle n_2\rangle$ denotes the longitudinally averaged value of $n_2(x)$, then equation **Error! Reference source not found.** simplifies giving P_f in terms of P_i,

$$P_f = P_i e^{[\eta_{ol}(\sigma_{em}-\sigma_{ESA})n_2(x)-\alpha_{BG}]2l_f} \quad (5)$$

and does not require any information regarding the longitudinal distribution of the population $n_2(x)$, only its longitudinally averaged value. If the laser is operating in steady-state then

$$P_f R_{oc} = P_i \quad (6)$$

because the intracavity power after making a roundtrip must return to its initial value in steady state operation. Substituting equation **Error! Reference source not found.** into **Error! Reference source not found.** gives the following equation

$$P_f = P_i R_{oc} e^{[\eta_{ol}(\sigma_{em}-\sigma_{ESA})\langle n_2\rangle-\alpha_{BG}]2l_f} \quad (7)$$

which if P_f is nonzero requires

$$1 = R_{oc} e^{[\eta_{ol}(\sigma_{em}-\sigma_{ESA})\langle n_2\rangle-\alpha_{BG}]2l_f} \quad (8)$$

Solving **Error! Reference source not found.** for $\langle n_2\rangle$ gives

$$\langle n_2\rangle = \frac{\frac{1}{2l_f}\ln\left(\frac{1}{R_{oc}}\right)+\alpha_{BG}}{\eta_{ol}(\sigma_{em}-\sigma_{ESA})} \quad (9)$$

which is the value at which the longitudinally averaged $^4F_{3/2}$ population is pinned if the intracavity laser power is nonzero. Using power balance, we now derive an equation for the output laser power by requiring the absorbed pump power be equal to the sum of the powers in these various channels. For the present system, this statement of power balance is

$$P_{\substack{pump\\abs}} = P_{laser} + P_{thermal} + P_{fluorescence} + P_{\substack{loss\\ESA}} + P_{\substack{loss\\BG}} \quad (10)$$

With our goal being an expression for the output laser power in terms of experimentally known laser parameters, we now calculate the various flow-down channels for the absorbed pump power given in **Error! Reference source not found.**. The presence of non-radiative decays in the laser system is accounted for by $P_{thermal}$ in **Error! Reference source not found.**. We partition $P_{thermal}$ into three independent terms. Figure 1 shows the low-lying energy levels of Nd^{3+}, the pump and laser transitions, and the three groups of non-radiative transitions that contribute to the thermal load in the laser as detailed here:

Pump QD – The thermal load due to the pump photon quantum defect associated with populating the $^4F_{3/2}$ initial laser level and specifically due to $^4F_{5/2}$ to $^4F_{3/2}$ non-radiative transitions.

Laser QD – The thermal load due to the laser photon quantum defect associated with de-populating the $^4I_{13/2}$ terminal laser level and specifically due to the $^4I_{13/2}$ to $^4I_{9/2}$ non-radiative transitions.

Fluorescence QD – The thermal load due to fluorescent photon quantum defects associated with depopulating the terminal fluorescent transition levels and specifically due to the $^4I_{15/2}$, $^4I_{13/2}$ and $^4I_{11/2}$ to $^4I_{9/2}$ non-radiative transitions.

Separately calling out these three thermal channels recasts the power balance equation **Error! Reference source not found.** as

$$P_{\substack{pump\\abs}} = P_{laser} + P_{\substack{thermal\\pump\ QD}} + P_{\substack{thermal\\laser\ QD}} + P_{\substack{thermal\\fluorescence\ QD}} + P_{fluorescence} + P_{\substack{loss\\ESA}} + P_{\substack{loss\\BG}} \quad (11)$$

where the various terms in **Error! Reference source not found.** are defined in Table I.

Table I Absorbed Pump Power Flow Down Channels

Terms in Power Balance Equation Error! Reference source not found.	**Comment**
$\boldsymbol{P_{\substack{pump\\absorbed}} = \eta_{del} P_{pump} \times \left(1 - e^{-\frac{A_{core}}{A_{clad}}\langle n_1\rangle \sigma_{abs} \frac{l_f}{2}}\right)}$	Absorbed pump power
$\boldsymbol{P_{\substack{thermal\\pump\ QD}} = P_{\substack{pump\\absorbed}} \left(1 - \frac{\lambda_{pump}}{\lambda_{^4F_{3/2}-{}^4I_{9/2}}}\right)}$	Thermal power from pump QD
$\boldsymbol{P_{\substack{thermal\\laser\ QD}} = \frac{R_{OC}}{1-R_{OC}} P_{laser} \times \frac{e^{[\eta_{ol}(\sigma_{em}-\sigma_{ESA})\langle n_2\rangle-\alpha_{BG}]\,2l_f} - 1}{\eta_{ol}(\sigma_{em}-\sigma_{ESA})\langle n_2\rangle - \alpha_{BG}} \times \eta_{ol}\sigma_{em}\langle n_2\rangle \left(\frac{\lambda_{laser}}{\lambda_{^4F_{3/2}-{}^4I_{9/2}}} - 1\right)}$	Thermal power from laser QD
$\boldsymbol{P_{\substack{thermal\\fluorescence\ QD}} = \frac{\langle n_2\rangle A_{core} l_f}{\tau_2} \times \left(\frac{hc}{\lambda_{^4F_{3/2}-{}^4I_{9/2}}} - \frac{hc}{\langle\lambda_{fluorescence}\rangle}\right)}$	Thermal power from Fluorescence QD

$P_{fluorescence} = \frac{\langle n_2 \rangle A_{core} l_f}{\tau_2} \times \frac{h c}{\langle \lambda_{fluorescence} \rangle}$	Fluorescence power emitted from laser gain core
$P_{\underset{ESA}{loss}} \approx \frac{R_{OC}}{1 - R_{OC}} P_{laser} \times \frac{e^{[\eta_{ol}(\sigma_{em}-\sigma_{ESA})\langle n_2\rangle - \alpha_{BG}]\, 2 l_f} - 1}{\eta_{ol}(\sigma_{em}-\sigma_{ESA})\langle n_2\rangle - \alpha_{BG}} \eta_{ol} \sigma_{ESA} \langle n_2 \rangle$	Intracavity laser power lost to ESA
$P_{\underset{BG}{loss}} \approx \frac{R_{OC}}{1 - R_{OC}} P_{laser} \frac{e^{[\eta_{ol}(\sigma_{em}-\sigma_{ESA})\langle n_2\rangle - \alpha_{BG}]\, 2 l_f} - 1}{\eta_{ol}(\sigma_{em}-\sigma_{ESA})\langle n_2\rangle - \alpha}$	Intracavity laser background absorption and scattering

Note that $\langle n_2 \rangle$, the $^4F_{3/2}$ longitudinally averaged population in Table I is given in terms of known laser parameters by equation **Error! Reference source not found.** and further constrained by

$$\langle n_1 \rangle + \langle n_2 \rangle = n_0 \tag{12}$$

where $\langle n_1 \rangle$ is the $^4I_{9/2}$ longitudinally average population and n_0 is the Nd^{3+} density in the fiber core. Also note that in the expression for $P_{\underset{fluorescence\ QD}{thermal}}$, $\langle \lambda_{fluorescence} \rangle$ is the average wavelength of all the fluorescent photons from the $^4F_{3/2}$ level. Using the known branching ratios of the $^4F_{3/2}$ level listed in Table II, $\langle \lambda_{fluorescence} \rangle$ is calculated to be ~1019 nm.

Table II Branching Ratios of Nd^{3+} $^4F_{3/2}$ Transitions

Transition	Branching ratio[1]	Mean wavelength
$^4F_{3/2} \rightarrow {}^4I_{15/2}$	0.004	1960 nm
$^4F_{3/2} \rightarrow {}^4I_{13/2}$	0.09	1370 nm
$^4F_{3/2} \rightarrow {}^4I_{11/2}$	0.48	1064 nm
$^4F_{3/2} \rightarrow {}^4I_{9/2}$	0.43	877 nm

[1]Branching ratios obtained from Jacobs and Weber [9]

Here we give a brief discussion and derivation of some of the terms in Table I. The terms $P_{\underset{abs}{pump}}$, $P_{\underset{pump\ QD}{thermal}}$, $P_{\underset{fluorescence\ QD}{thermal}}$ and $P_{fluorescence}$ are self-explanatory, but the terms $P_{\underset{pump\ QD}{thermal}}$, $P_{\underset{ESA}{loss}}$ and $P_{\underset{BG}{loss}}$ involve some level of approximation and so deserve discussion. For $P_{\underset{ESA}{loss}}$, at any location x in the fiber, the loss in intracavity laser power per unit length due to ESA is given by

$$\frac{dP_{\underset{ESA}{loss}}}{dx} = P(x)\eta_{ol}\sigma_{ESA}n_2(x) \approx P(x)\eta_{ol}\sigma_{ESA}\langle n_2 \rangle \tag{13}$$

where we have approximated the right-hand side of the above equation with the substitution $n_2(x) \rightarrow \langle n_2 \rangle$. Integrating **Error! Reference source not found.** over a roundtrip through the fiber then gives

$$P_{\underset{ESA}{loss}} \approx \left(\int_0^{2l_f} P(x)\, dx \right) \eta_{ol}\sigma_{ESA}\langle n_2 \rangle \tag{14}$$

Approximating the integral over the fiber roundtrip in **Error! Reference source not found.** using

$$P(x) \approx P_i e^{[\eta_{ol}(\sigma_{em}-\sigma_{ESA})\langle n_2\rangle - \alpha_{BG}]} \tag{15}$$

which is itself an approximation because of the approximation $n_2(x) \rightarrow \langle n_2 \rangle$ invoked in **Error! Reference source not found.** then gives

$$\int_0^{2l_f} P(x)\, dx \approx \int_0^{2l_f} P_i e^{[\eta_{ol}(\sigma_{em}-\sigma_{ESA})\langle n_2\rangle - \alpha_{BG}]x}\, dx = P_i \frac{e^{[\eta_{ol}(\sigma_{em}-\sigma_{ESA})\langle n_2\rangle - \alpha_{BG}]} - 1}{[\eta_{ol}(\sigma_{em}-\sigma_{ESA})\langle n_2\rangle - \alpha_{BG}]} \tag{16}$$

On substitution of the right-hand side of **Error! Reference source not found.** back into **Error! Reference source not found.** gives

$$P_{\underset{ESA}{loss}} \approx \frac{R_{oc}}{1-R_{oc}} P_{laser} \frac{e^{[\eta_{ol}(\sigma_{em}-\sigma_{ESA})\langle n_2\rangle - \alpha_{BG}]} - 1}{[\eta_{ol}(\sigma_{em}-\sigma_{ESA})\langle n_2\rangle - \alpha_{BG}]} \eta_{ol}\sigma_{ESA}\langle n_2 \rangle \tag{17}$$

where we have additionally re-written P_i in terms of P_{laser} (see Figure 1) using

$$P_i = \frac{R_{oc}}{1-R_{oc}} P_{laser} \tag{18}$$

Following an analogous development for the calculation of the intracavity laser power lost to background absorption and scattering on a round trip through the fiber gives

$$P_{\underset{BG}{loss}} \approx P_1 \frac{e^{[\eta_{ol}(\sigma_{em}-\sigma_{ESA})\langle n_2\rangle - \alpha_{BG}]} - 1}{[\eta_{ol}(\sigma_{em}-\sigma_{ESA})\langle n_2\rangle - \alpha_{BG}]} \alpha_{BG} \tag{19}$$

To calculate the $P_{\underset{pump\ QD}{thermal}}$ term in equation **Error! Reference source not found.** we note that every laser photon emitted in the laser cavity generates an accompanying amount of heat given by

$$\Delta Q_{\,{}^4I_{\frac{13}{2}} - {}^4I_{\frac{9}{2}}} = \frac{hc}{\lambda_{\,{}^4F_{\frac{3}{2}} - {}^4I_{\frac{9}{2}}}} - \frac{hc}{\lambda_{laser}} = \frac{hc}{\lambda_{laser}} \left(\frac{\lambda_{laser}}{\lambda_{\,{}^4F_{\frac{3}{2}} - {}^4I_{\frac{9}{2}}}} - 1 \right) \tag{20}$$

due to the $^4I_{13/2}$-$^4I_{9/2}$ non-radiative transition that follows the generation of each laser photon. Following an analogous development to that used to derive the $P_{\underset{ESA}{loss}}$ term, the following rate gives the number of laser photons generated per unit time inside the laser cavity

$$\Gamma_{\underset{photons}{laser}} = \frac{R_{oc}}{1-R_{oc}} \frac{P_{laser}}{hc/\lambda_{laser}} \frac{e^{[\eta_{ol}(\sigma_{em}-\sigma_{ESA})\langle n_2\rangle - \alpha_{BG}]} - 1}{[\eta_{ol}(\sigma_{em}-\sigma_{ESA})\langle n_2\rangle - \alpha_{BG}]} \eta_{ol}\sigma_{em}\langle n_2 \rangle \tag{21}$$

or equivalently the stimulated emission rate of laser photons inside the laser cavity. Multiplying the right hand side of **Error! Reference source not found.** by the thermal energy given in **Error! Reference source not found.** then gives the rate of thermal energy dissipated in the laser cavity due to the $^4I_{13/2}$-$^4I_{9/2}$ non-radiative transition that follows the generation of each laser photon

$$P_{\underset{laser\ QD}{Thermal}} = \frac{R_{oc}}{1-R_{oc}} P_{laser} \frac{e^{[\eta_{ol}(\sigma_{em}-\sigma_{ESA})\langle n_2\rangle - \alpha_{BG}]} - 1}{[\eta_{ol}(\sigma_{em}-\sigma_{ESA})\langle n_2\rangle - \alpha_{BG}]} \eta_{ol}\sigma_{em} \times \langle n_2 \rangle \left(\frac{\lambda_{laser}}{\lambda_{\,{}^4F_{\frac{3}{2}} - {}^4I_{\frac{9}{2}}}} - 1 \right) \tag{22}$$

The development of an expression for $P_{\underset{abs}{Pump}}$ follows similar reasoning to that used above. The total pump power lost in the fiber due to both useful absorption and background loss is given by

$$\eta_{del} P_{pump} \left(1 - e^{-(\eta_{ol\,pump}\sigma_{ESA}\langle n_2\rangle + \alpha_{BG})\frac{l_f}{2}}\right) \tag{23}$$

where α_{BG} is the background loss of pump light in the fiber which we here assume is the same as for the laser light, σ_{abs} is the pump light absorption cross section in the fiber, and $\eta_{ol\,pump}$ $\eta_{ol\ pump}$ is the pump irradiance profile overlap with the doped absorbing core of the fiber. The reason for the factor of $l_f/2$ in the exponential of expression **Error! Reference source not found.** is that the injected pump light only traverses half the fiber length before exiting the fiber. To calculate the fraction of pump power that is usefully absorbed in the fiber multiply the total pump loss given by **Error! Reference source not found.** by the factor

$$\frac{\eta_{ol\,pump}\langle n_1\rangle\sigma_{abs}}{\eta_{ol\,pump}\langle n_1\rangle\sigma_{abs} + \alpha_{BG}} \tag{24}$$

giving

$$P_{\substack{pump \\ abs}} = \eta_{del} P_{pump} \frac{1 - e^{-\left(\eta_{ol\,pump}\langle n_1\rangle\sigma_{abs} + \alpha_{BG}\right)\frac{l_f}{2}}}{\eta_{ol\,pump}\langle n_1\rangle\sigma_{abs} + \alpha_{BG}} \eta_{ol\,pump}\langle n_1\rangle\sigma_{abs} \tag{25}$$

for the usefully absorbed pump light. Solving for the output laser power, P_{laser} using **Error! Reference source not found.** is now straight forward. Substituting for the terms on the right-hand side of **Error! Reference source not found.** using the expressions for these terms given in Table I gives

$$P_{laser} = \frac{\frac{\lambda_{pump}}{\lambda_{{}^4F_{\frac{3}{2}} - {}^4I_{\frac{9}{2}}}}\left(P_{\substack{pump \\ absorbed}} - \frac{\langle n_2\rangle A_{core} l_f}{\tau_2}\frac{hc}{\lambda_{pump}}\right)}{1 + \left(\frac{R_{OC}}{1-R_{OC}}\right)\left(\frac{e^{\left[\eta_{ol}(\sigma_{em} - \sigma_{ESA})\langle n_2\rangle - \alpha_{BG}\right]2l_f} - 1}{\eta_{ol}(\sigma_{em} - \sigma_{ESA})\langle n_2\rangle - \alpha_{BG}}\right)} \times \frac{1}{\left(\eta_{ol}\sigma_{em}\langle n_2\rangle\left(\frac{\lambda_{laser}}{\lambda_{{}^4F_{\frac{3}{2}} - {}^4I_{\frac{9}{2}}}} - 1\right) + \eta_{ol}\sigma_{em}\langle n_2\rangle + \alpha_{BG}\right)} \tag{26}$$

Equation **Error! Reference source not found.** immediately gives the familiar looking result

$$P_{laser} = \eta_{slope}\left(P_{\substack{pump \\ abs}} - P_{\substack{pump \\ threshold}}\right) \tag{27}$$

Examining **Error! Reference source not found.**, the laser slope efficiency, η_{slope} , and absorbed pump power at lasing threshold, $P_{\substack{pump \\ threshold}}$, are given by

$$\eta_{slope} = \frac{\frac{\lambda_{pump}}{\lambda_{{}^4F_{\frac{3}{2}} - {}^4I_{\frac{9}{2}}}}}{1 + \left(\frac{R_{OC}}{1-R_{OC}}\right)\left(\frac{e^{\left[\eta_{ol}(\sigma_{em} - \sigma_{ESA})\langle n_2\rangle - \alpha_{BG}\right]2l_f} - 1}{\eta_{ol}(\sigma_{em} - \sigma_{ESA})\langle n_2\rangle - \alpha_{BG}}\right)} \times \frac{1}{\left(\eta_{ol}\sigma_{em}\langle n_2\rangle\left(\frac{\lambda_{laser}}{\lambda_{{}^4F_{\frac{3}{2}} - {}^4I_{\frac{9}{2}}}} - 1\right) + \eta_{ol}\sigma_{em}\langle n_2\rangle + \alpha_{BG}\right)} \tag{28}$$

and

$$P_{\substack{pump \\ threshold}} = \frac{\langle n_2\rangle A_{core} l_f}{\tau_2}\frac{hc}{\lambda_{pump}} \tag{29}$$

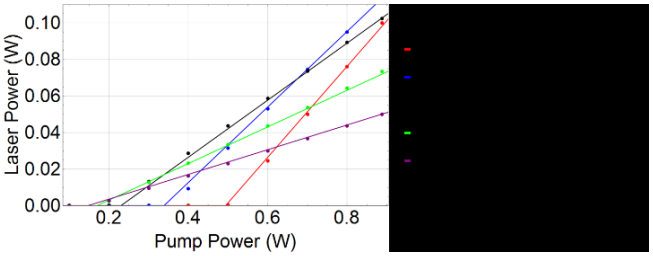

Although the development of the longitudinally averaged population model pursued here was for the specific case of a Nd^{3+} fiber laser operating on its ${}^4F_{3/2}$-${}^4I_{13/2}$ transition, the technique itself is quite general and applicable to other lasant species having different spectroscopy's and different parasitic kinetic processes. What is required is that an energy balance equation such as **Error! Reference source not found.** be developed as we have done in the foregoing example.

3. RESULTS

Using equation (26) for the laser output power we are now in a position to demonstrate the usefulness of the laser model by applying it to the analysis of our laser data. Specifically, we will fit our model to the experimental laser output power vs pump power data shown in Fig. 3. The goal of this exercise is to find a single set of model parameters that faithfully replicate the data over the entire parameter space investigated experimentally. The data of figure 3 was taken using two different configurations. In the case of the 0.04 reflectivity output coupler the uncoated facet of the fiber served as the OC. In the four other cases shown an external output coupler was additionally used after the uncoated fiber facet. For the cases in which external output couplers were used the reflectivities listed in figure 3 correspond to the measured reflectance's of those optics. It is important to note that in cases using an external output coupler the effective reflectivity seen by the laser can be different than the measured reflectivity value of standalone output coupler. In these cases, the reflectivity seen by the laser can depend on both the Fresnel reflectivity of the uncoated fiber facet and the reflectivity of the external optic because these two surface reflections can be coherently coupled by the laser radiation, i.e., the combination of the Fresnel reflectivity of the uncoated fiber facet and the reflectivity of the external output coupler behave as a Fabry-Perot etalon. In this case the effective reflectivity seen by the laser is

$$R_{Eff} = \left[\frac{-\sqrt{R_F} + e^{2i\delta}(1-R_F)\sqrt{R_{oc}} + e^{2i\delta}R_F\sqrt{R_{oc}}}{-1 + e^{2i\delta}\sqrt{R_F}\sqrt{R_{oc}}}\right] \tag{30}$$

where R_F is the Fresnel reflectivity of the uncoated fiber facet, R_{oc} is the reflectivity of the standalone external output coupler and δ is the one-way phase delay between the fiber output facet and the external output coupler surface

$$\delta = 2\pi\frac{l_{facet-oc}}{\lambda_{laser}} \tag{31}$$

where $l_{facet-oc}$ is the spatial separation between the two surfaces. Depending on the value of δ, the effective reflectivity **Error! Reference source not found.** can swing between a minimum value of

$$R_{Eff,\min} = \left(\frac{\sqrt{R_{oc}} - \sqrt{R_F}}{1 - \sqrt{R_{oc}R_F}}\right)^2 \tag{32}$$

and a maximum value of

Model Parameter	Value	Description
l_F	1400 cm	Length of the gain loaded portion of fiber
λ_{Pump}	808 nm	Pump wavelength
λ_{Laser}	1400 nm	Laser wavelength
$\lambda_{^4F_{3/2}-^4I_{9/2}}$	~877 nm	Wavelength of $^4F_{3/2}$-$^4I_{9/2}$ transition
$\langle\lambda_{Fluorescence}\rangle$	1019 nm	Average wavelength of fluorescence out of the $^4F_{3/2}$ level
τ_2	450 μs	Fluorescent lifetime of the $^4F_{3/2}$ level
σ_{em}	0.23x10^{-20} cm^2	Laser stimulated emission cross section
σ_{esa}	0.098x10^{-20} cm^2	Laser excited state absorption cross section
σ_{Pump}	1.16x10^{-20} cm^2	Pump absorption cross section
n_0	4.2x10^{18}/cm^3	Nd^{3+} doping density
η_{Del}	1	Delivery efficiency of the pump into the fiber
$\eta_{ol\ laser}$	0.508	Overlap of laser irradiance profile with the gain core of the fiber
$\eta_{ol\ pump}$	0.704	Overlap of pump irradiance profile with the gain core of the fiber
α_{BG}	0.00034/cm for cases using external OCs 0.0002/cm for case using uncoated fiber cleave as OC	Background scatter and absorption loss
A_{Core}	3.42x10^{-7} cm^2	Area of the doped core of the fiber

$$R_{Eff,max} = \left(\frac{\sqrt{R_{OC}}+\sqrt{R_f}}{1+\sqrt{R_{OC}R_f}}\right)^2 \quad (33)$$

However, for the presently considered case the precise wavelength of the laser is not constrained allowing the value of to change as the wavelength of the laser changes. Taking this into account, the expectation is that the laser system will self-adjust its wavelength to have an effective reflectivity near $R_{Eff,max}$, thus minimizing the threshold pump power. In fitting or our model to the experimental data, for those cases that used an external output coupler we will allow the effective reflectivity of the system to vary within the boundaries given by (32) and (33), respectively.

Figure 5: Overlay of model projections on the experimental data from figure 3. In those cases that used an external output coupler, R_{Eff} is treated as a fit parameter constrained by the minimum and maximum reflectivity values given by equations **Error! Reference source not found.** and **Error! Reference source not found.**, respectively, and as listed in plot legend. The specific values of the other model parameters used in the fit are given in Table III. In all cases the fit value for the effective reflectivity is at or very near the maximum reflectivity value allowed by equation **Error! Reference source not found.**. This is as expected because the system self-adjusts its wavelength to minimize its lasing threshold.

Figure 5 shows the modeling fit to plotted data for the laser output power as a function of the pump power applied. The 0.04 output coupler reflectivity corresponds to using the uncoated fiber facet as the output coupler. All other cases use an external output coupler after the uncoated fiber facet having the indicated measured reflectivity. In those cases that used an external output coupler, R_{eff} is treated as a fit parameter constrained by the minimum and maximum reflectivity values given by equations (32) and (33), respectively, and as listed in plot legend. The specific values of the other model parameters used in the fit are given in Table III.

Table III Summary of Model Parameters and Values

Table III summarizes the parameters used in our model and the values we have found that give the best fit of our model to the slope efficiency data by eye. The total length of active fiber in the gain module is 14 m, in two 7 m lengths. The pump wavelength is 808 nm. Both pump absorption cross-section and doping density are obtained from a measurement of losses at the pump wavelength. The laser emission wavelength is 1400 nm. The average fluorescence wavelength is determined by using published branching ratio values for the radiative transitions out of the $^4F_{3/2}$ state [9]. The fluorescence lifetime was taken to be 450 μs from a published valued measured in a fiber of a similar glass composition [13]. The emission cross section was calculated from a measurement of the fluorescence from a small piece of the doped glass cane. The area of the doped region was calculated considering un-doped silica regions that are introduced in homogenization. The overlap factors for the pump field and the laser field with the doped region was determined by modeling the space-filling mode at both wavelengths in COMSOL. It is assumed that all the pump power is delivered to the gain fiber, i.e. a pump deliver efficiency of 1. The parameters that are left adjustable in the fit are the overall system background losses and the ESA cross section. The case where the Fresnel reflection from the fiber end was used as the output coupler was treated separately from the case where a free-space coupler was used as an output coupler. For external output couplers, the cavity loss was allowed to increase to account for the increased transmission losses due to imperfect feedback into the fiber from the output coupler reflection.

A. Emission cross section $^4F_{3/2}$ to $^4I_{13/2}$

The value of the emission cross-section at the laser wavelength obtained from this model differs from what we calculate from a fluorescence measurement [12]. The calculation was obtained from a measurement of the spontaneous fluorescence of the core material alone. We have allowed for both the emission and ESA cross section values to shift in fitting this model to the data. The obtained correction to these values was a 15% increase.

B. Power conversion flow down

It is instructive using the power balance terms of Table I to see how the pump power absorbed by the laser system partitions itself between the various channels that are open to it. The bar graph in figure 6 (a) shows the amount of power that flows down into various channels of which the laser power is a lesser but significant portion. The model allows for quick evaluation of important performance considerations such as heating from non-radiative transitions and expected laser output power.

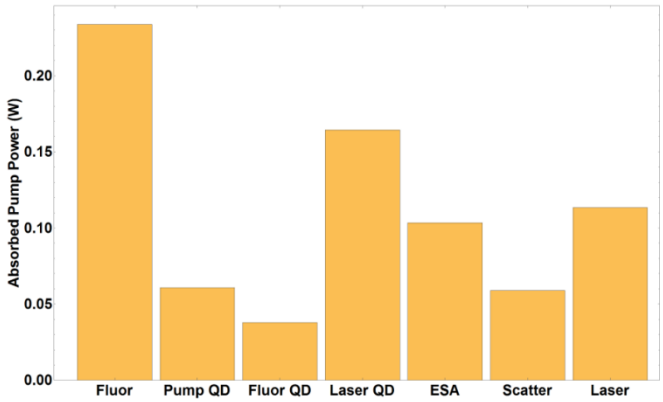

Figure 6: (a) Bar graph shows the amount of power that flows down into various channels for the case where the effective reflectivity is 0.16. About 13% of the absorbed pump power is converted to laser power. This analysis allows for quick evaluation of important performance considerations such as heating from non-radiative transitions and expected laser output power.

Despite the vastly improved performance of this fiber laser over previous work, excess scattering, excited state absorption and excess OH absorption degrade the laser performance here. The modeling enables us to project fabrication improvements to this fiber. From the power flow into various channels shown in figure 6, it is evident that significant amount of pump power is lost to scattering in this fiber. We believe that the losses due to scattering and OH absorption exceed the lowest possible due to contamination during the fabrication process.

At threshold, the fraction of the pump power that converts to fluorescence is at a maximum. Increasing the pump power beyond that promotes lasing while the fluorescence power stays fixed, thus pumping harder increases efficiency. Power lost to excited state absorption can be suppressed by judicious choice of host glass composition. Dopants like aluminum, germanium or phosphorous or network modifiers like Li_2O, Na_2O, K_2O could expand the tunable range and increase the maximum achievable gain [14]. A future fiber with such a composition and processing improvements would reduce these inhibitors allowing for more pump power to be distributed into other channels thus improving the laser output power performance at 1400 nm.

Processing improvements would reduce these inhibitors allowing for more pump power to be distributed into other channels thus improving the laser output power performance. Additionally, power lost to excited state absorption can be suppressed by judicious choice of host glass composition. A future fiber with such a composition could realize substantial improvement of laser power on the 1400 nm line.

4.DISCUSSION

This model allows for quick analysis of fiber laser performance which is particularly useful, for example in prediction of cost per watt of output power. In the case of the Nd^{3+} filtering fiber we were able to apply the model to output powers measured as a function of pumping power and as a function of output coupler reflectivity. This is a classic 4-level laser and application of the model to a 3-level laser is straightforward [15].

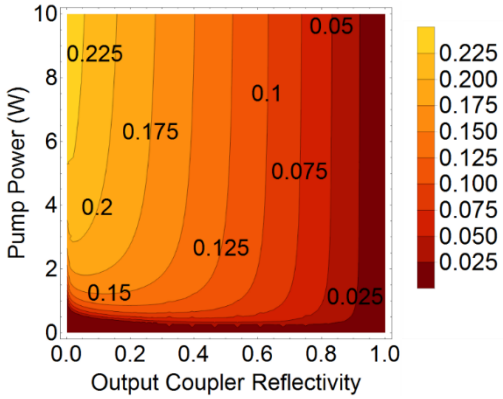

Figure 7: Contour plot showing modeled curves of constant optical to optical efficiency (η_{o-o}) for various pumping powers and output coupler reflectivities. The maximum efficiency approaching 25% occurs for small output coupling and high pumping powers This agrees well with our obtained efficiency of 26% for a low reflectivity output coupling.

We recognize that the 15% difference in emission cross-section and the 32% difference in the ESA cross-section values between this work and our prior work is significant. However, study of this laser transition in this glass composition is to our knowledge limited to our work here on this single fiber example. There are several parameters in our work that are not well known such as exact ion concentration, exact upper state lifetime, mode field diameter, distribution of the gain ions within the fiber structure and overlap integral between the gain and the laser and pump modes. We have to date not been able to resolve all sources of error and it is likely additional work on additional fibers will be required to more tightly restrict the range of the emission cross-section and the excited state absorption cross section of Nd^{3+} at these wavelengths.

Fiber lasers with microstructure filtering could impact many application spaces as the fiber laser architecture is best suited for power scaling [16]. In particular, an optical fiber maintains constant beam diameter as a function of length and is capable of attaining low scattering and absorption losses creating a platform for extremely long, high intensity optical interactions which in turn allow fiber lasers to utilize low gain laser transitions not accessible to free-space pumped configurations. The addition of wavelength selective losses to the toolset expands this feature by allowing a designer to consider laser ions with multiple transitions and use the structure to suppress stronger transitions in favor of even weaker transitions. In fact in the case of Nd^{3+} we have shown that the 1400 nm transition that has effectively no gain when the 1064 nm transition is not suppressed can be turned into a relatively high gain, efficient laser when the 1064 nm line is suppressed. It is likely this scheme can be applied to other well-known multi-transition laser ions with non-zero gain in silica [17]. Nonlinear frequency conversion can be leveraged to span an even greater range of wavelengths.

This also presents an opportunity to increase the wall-plug efficiency in bands where sources exist as with Nd^{3+} lasers for in this transition which are typically Nd:YAG. Bulk lasers, such as Nd:YAG, are limited in efficiency by relatively lower consumption of pumping power. Replacing these systems with fiber lasers present an opportunity to

increase efficiency with a cost-effective method that produces high output power and good beam quality. Our model here shows a pathway to further increase of the amplification efficiency of the 1400 nm line via reduction in scattering and background losses. The ultimate limitation on efficiency is set by the wall-plug efficiency of the diode pumps and the quantum efficiency of the laser transition.

In conclusion, we have demonstrated a simplified model capable of predicting fiber laser performance in a microstructure filtering optical fiber that operates on a non-standard transition for Nd^{3+} in silica. This model can be generally extended to fiber laser systems for rapid analysis of laser performance and limitations.

Funding sources and acknowledgments. funding was provided by LLNL's Innovation Development Fund, through the Innovation & Partnerships Office . This work was performed under the auspices of the U.S. Department of Energy by Lawrence Livermore National Laboratory under Contract DE-AC52-07NA27344. LLNL-JRNL-753963.

Acknowledgment. The authors would like to thank Dr. Charles Boley, Dr. Alexander Rubenchik and Dr. Christopher Ebbers for several helpful discussions and Benjamin Pyke for his helpful spectrometer measurements.

References

1. L. Shien-Kuei, and C. Yung-Kuang, "Passive gain-equalized wide-band erbium-doped fiber amplifier using samarium-doped fiber," IEEE Photonics Technology Letters **8**, 879-881 (1996).
2. S. Kawakami, and S. Nishida, "Characteristics of a doubly clad optical fiber with a low-index inner cladding," IEEE Journal of Quantum Electronics **10**, 879-887 (1974).
3. D. B. S. Soh, Y. Seongwoo, J. Nilsson, J. K. Sahu, O. Kyunghwan, B. Seungin, J. Yoonchan, C. Codemard, P. Dupriez, K. Jaesun, and V. Philippov, "Neodymium-doped cladding-pumped aluminosilicate fiber laser tunable in the 0.9-μm wavelength range," IEEE Journal of Quantum Electronics **40**, 1275-1282 (2004).
4. W. J. Miniscalco, L. J. Andrews, B. A. Thompson, R. S. Quimby, L. J. B. Vacha, and M. G. Drexhage, "1.3 mu m fluoride fibre laser," Electronics Letters **24**, 28-29 (1988).
5. T. Komukai, Y. Fukasaku, T. Sugawa, and Y. Miyajima, "Highly efficient and tunable Nd^{3+} doped fluoride fibre laser operating in 1-3 mu m band," Electronics Letters **29**, 755-757 (1993).
6. A. A. Kaminskii, *Laser Crystals: Their Physics and Properties* (Springer Berlin Heidelberg, 2013).
7. D. Krennrich, R. Knappe, B. Henrich, R. Wallenstein, and J. A. L'huillier, "A comprehensive study of Nd: YAG, Nd: YAlO 3, Nd: YVO 4 and Nd: YGdVO 4 lasers operating at wavelengths of 0.9 and 1.3 μm. Part 1: cw-operation," Applied Physics B **92**, 165 (2008).
8. H. Zhu, C. Huang, G. Zhang, Y. Wei, L. Huang, J. Chen, W. Chen, and Z. Chen, "High-power CW diode-side-pumped 1341 nm Nd: YAP laser," Optics communications **270**, 296-300 (2007).
9. R. Jacobs, and M. Weber, "Dependence of the $^4F_{3/2} \rightarrow {}^4I_{11/2}$ induced-emission cross section for Nd^{3+} on glass composition," IEEE Journal of Quantum Electronics **12**, 102-111 (1976).
10. I. P. Alcock, A. I. Ferguson, D. C. Hanna, and A. C. Tropper, "Tunable, continuous-wave neodymium-doped monomode-fiber laser operating at 0.900–0.945 and 1.070–1.135 μm," Optics Letters **11**, 709-711 (1986).
11. P. H. Pax, V. V. Khitrov, D. R. Drachenberg, G. S. Allen, B. Ward, M. Dubinskii, M. J. Messerly, and J. W. Dawson, "Scalable waveguide design for three-level operation in Neodymium doped fiber laser," Optics express **24**, 28633-28647 (2016).
12. J. W. Dawson, L. S. Kiani, P. H. Pax, G. S. Allen, D. R. Drachenberg, V. V. Khitrov, D. Chen, N. Schenkel, M. J. Cook, R. P. Crist, and M. J. Messerly, "E-band Nd3+ amplifier based on wavelength selection in an all-solid micro-structured fiber," Optics Express **25**, 6524-6538 (2017).
13. C. Bartolacci, M. Laroche, T. Robin, B. Cadier, S. Girard, and H. Gilles, "Effects of ions clustering in Nd^{3+}/Al^{3+}-codoped double-clad fiber laser operating near 930 nm," Applied Physics B **98**, 317-322 (2010).
14. H. G. Lipson, J. R. Buckmelter, and C. O. Dugger, "Neodymium ion environment in germanate crystals and glasses," Journal of Non-Crystalline Solids **17**, 27-43 (1975).
15. R. J. Beach, W. F. Krupke, V. K. Kanz, S. A. Payne, M. A. Dubinskii, and L. D. Merkle, "End-pumped continuous-wave alkali vapor lasers: experiment, model, and power scaling," Journal of the Optical Society of America B **21**, 2151-2163 (2004).
16. J. W. Dawson, M. J. Messerly, R. J. Beach, M. Y. Shverdin, E. A. Stappaerts, A. K. Sridharan, P. H. Pax, J. E. Heebner, C. W. Siders, and C. P. J. Barty, "Analysis of the scalability of diffraction-limited fiber lasers and amplifiers to high average power," Optics Express **16**, 13240-13266 (2008).
17. B. J. Ainslie, S. P. Craig, and S. T. Davey, "The absorption and fluorescence spectra of rare earth ions in silica-based monomode fiber," Journal of Lightwave Technology **6**, 287-293 (1988).